

Raman Scattering from High Frequency Phonons in Supported n-Graphene Layer Films

A. Gupta^a, Gugang Chen^a, P. Joshi^b, S. Tadigadapa^b and P.C. Eklund^{a,c}

^a Department of Physics, ^b Electrical Engineering

^c Materials Research Institute and Department of Materials Science and Engineering

The Pennsylvania State University, University Park, PA 16802 USA

ABSTRACT

Results of room temperature Raman scattering studies of ultrathin graphitic films supported on Si (111)/SiO₂ substrates are reported. The results are significantly different from those known for graphite. Spectra were collected using 514 nm radiation on films containing from n=1 to 20 graphene layers, as determined by atomic force microscopy. Both the 1st and 2nd order Raman spectra show unique signatures of the number of layers in the film. The nGL film analog of the Raman G-band in graphite exhibits a Lorentzian lineshape whose center frequency shifts linearly relative to graphite as $\sim 1/n$ (for n=1 $\omega_G \sim 1588 \text{ cm}^{-1}$). Three weak bands, identified with disorder-induced 1st order scattering, are observed at $\sim 1350, 1450$ and 1500 cm^{-1} . The 1500 cm^{-1} band is weak but relatively sharp and exhibits an interesting n-dependence. In general, the intensity of these D-bands decreases dramatically with increasing n. Three 2nd order bands are also observed ($\sim 2450, \sim 2700$ and 3248 cm^{-1}). They are analogs to those observed in graphite. However, the $\sim 2700 \text{ cm}^{-1}$ band exhibits an interesting and dramatic change of shape with n. Interestingly, for n<5 this 2nd order band is more intense than the G-band.

Several interesting reports of unusual electrical transport in ultra-thin graphite films have appeared recently ¹⁻¹⁵. These films are comprised of only a few atomic layers of sp²-bonded carbon known as “graphene” layers. Below, we refer to these unique atomically thin films as n-graphene layer films (i.e., *n*GL). Recently, bottom gate modulation of the current in the plane of the *n*GL film was also demonstrated which represents the first time that gate control of the current has been observed in a metallic or semi-metallic system ¹⁰. Interesting oscillatory magneto-transport phenomena sensitive to the shape of the Fermi surface ^{7, 8, 10, 12, 14-17} and an unusual half-integer Quantum Hall Effect ⁵ have been reported ^{7, 9, 16-18}.

Crystalline graphite is a strongly anisotropic layered solid consisting of a periodic ..ABAB.. stacking of graphene layers. All the formal chemical bonding in graphite is associated with the strong sp² intralayer bonds; these layers are, in turn, coupled by very weak van der Waals bonds. As a result of this strongly anisotropic bonding, weak (strong) electron and phonon dispersion is calculated ^{19, 20 21-31} and observed ^{32, 33} along the directions perpendicular (parallel) to the graphene planes. Any unique phonon character of *supported n*GL films is therefore expected to be due to the importance of the reduction and/or eventual loss of these interlayer forces (i.e., at *n*=1) and to a combination of weak charge transfer and/or strain associated with the coupling of the film to the substrate.

Phonon and electronic state dispersion in a single graphene layer has been studied theoretically for many years ³⁴⁻³⁶. In fact, these dispersion curves led to the prediction of chirality-dependent one-dimensional electronic and phonon dispersion in carbon

nanotubes²⁰. Experimental success in realizing well-ordered graphene (or n GLs) has been somewhat limited until very recently. A few years ago, a synthesis breakthrough was reported which is generally applicable to many layered solids that exhibit weak interlayer bonds (e.g., BN, NbSe₂)³⁷. The approach relies on the careful mechanical transfer of a thin section of material from the outer basal plane surface of a parent crystal to a supporting substrate. In one case, this was elegantly accomplished by mounting a small graphite crystal on a tip-less cantilever held in an atomic force microscope (AFM)¹⁰. Thin $n \sim 3$ n GLs have also been fabricated by the preferential thermal evaporation of Si from the (0001) surface of SiC in ultrahigh vacuum and they have been shown to also exhibit oscillatory magnetoresistance¹⁴.

Here we present the first formal report of our Raman scattering studies on n GLs, where n is in the range $1 < n < 20$, as determined by AFM³⁸. The films were made by mechanically transferring thin flakes of material from highly oriented pyrolytic graphite (HOPG) on to a reasonably smooth Si substrate. Despite the short range and weak interlayer forces within these films, we have observed a surprisingly continuous and systematic change in the 1st and 2nd order high frequency intralayer phonons as the number of layers n in the film increases. Raman scattering can therefore be used to identify the number of layers in an n GL film.

Our films were prepared as follows. Thin basal plane sections were removed from large slabs ($\sim 5 \times 5 \times 1 \text{ mm}^3$) of highly oriented pyrolytic graphite (HOPG)^{39, 40} by Scotch Tape (3M) and transferred to Si (111) substrates. These substrates have a ~ 100 nm thick thermally grown oxide overlayer, such as typically used for bottom gate control of nanotubes and nanowire devices^{41, 42}. An atomic force microscope (AFM; model XE

100, PSIA, Inc.) operating under ambient conditions was used to measure the surface roughness of the substrate ($\sim 1-2$ nm) and the apparent thickness of the various n GL films studied here. Typical minimum lateral dimensions of these n GLs usually exceeded $\sim 2-4$ μm . MicroRaman spectra could therefore be collected from a single n GL using a 100x objective with a spot size of ~ 1 μm . A variety of n GL flakes were deposited on a single Si substrate that was in turn mounted on the precision x - y translation stage of our Raman microscope. Raman spectra were then collected using 514.5 nm excitation under ambient conditions at low laser power (< 2 mW) using a JY-ISA T64000 triple holographic grating spectrometer with an LN₂ cooled CCD detector. A low-pressure Hg lamp (Oriel) was set up in the background to provide a reference frequency in all spectra that is present as a narrow line at 1122.5 cm^{-1} . The intrinsic resolution of the Raman spectrometer was also observed and recorded as the lineshape of this Hg line. Specific n GLs that had been previously characterized by AFM (film thickness and basal plane shape) could be recognized in the video display of the Raman microscope by their characteristic irregular shape. In this way, we were able to collect Raman spectra of n GL films of known thickness (n).

In Fig. 1, we plot the measured AFM thickness (h) vs. our assigned value for n . The straight line is the result of a linear least squares fit to the data. In making the tentative assignment for n , we assumed that the film would have a thickness given by the linear relation $h \sim n \cdot t + t_0$, where n is an integer (number of layers), t is the approximate theoretical thickness of a graphene layer, and t_0 is an instrumental offset (i.e., independent of n). The data for h in Fig. 1 represents the average step height obtained for a single n GL flake from averaging ~ 100 individual line scans using a Si AFM cantilever.

As can be seen, the linear fit to the $h(n)$ data is very good and we obtain $t=0.35 \pm 0.01$ nm, in good agreement with $c/2=0.335$ nm for graphite^{19, 20, 43}; the offset obtained is $t_0=0.33 \pm 0.05$ nm. We propose that t_0 may be the result, in part, of a different force of attraction between the tip and graphene, as compared to the tip with SiO₂. From the least squares fit, we find that the $n=1$ nGL has an apparent thickness of $h(1)=(t+t_0)=0.68 \pm 0.07$ nm.

In Fig. 2, we show a series of high frequency Raman spectra for nGLs of various n collected in a single experimental session. By this we mean that the spectra were collected in succession by only moving the x-y stage to position a new nGL flake under the microscope objective. The spectra in Fig. 2 cover the region ~ 1500 - 3600 cm⁻¹, and therefore contain contributions from both 1st order scattering, i.e., the G-band (~ 1582 cm⁻¹ in graphite) and also 2nd order scattering. The Raman spectra have been stacked in the figure from bottom to top according to increasing n ; the spectrum of HOPG ($n\sim 8$) appears on top. Furthermore, the intensity of each spectrum in Fig. 2 has been scaled to artificially produce the same strength 2nd order band near ~ 2700 cm⁻¹. If plotted in absolute Raman scattering intensity units (e.g., counts/watt-sec), the true G-band intensity in Fig. 2 would increase over the range $n=1$ to ~ 20 almost linearly with the number of layers in the nGL. In most of our experiments (passes), the G-band for HOPG is comparable in intensity to that of $n\sim 19$, suggesting that the optical penetration depth in the nGL is ~ 20 layers. Several general observations can easily be made from Fig. 2: (1) the G-band frequency downshifts with increasing n (for small n), (2) the 2nd order ~ 2700 cm⁻¹ band exhibits an interesting n -dependence in shape and frequency, (3) the sharp 2nd order feature at ~ 3248 cm⁻¹ is insensitive to n , (4) for $n<5$, the 2nd order ~ 2700 cm⁻¹ band

for an n GL is more intense than the 1st order G-band, and (5) additional weak features are present in the first order region ($\omega < 1620 \text{ cm}^{-1}$) (we show these later on an expanded intensity scale).

In Fig. 3, on an expanded frequency scale, we show the G-band for various n GLs. The spectra are stacked from bottom to top with increasing n . The spectra in the figure were also collected in a single pass, i.e., they were also collected sequentially under identical optical conditions. The Raman spectra in Fig. 3 are not scaled, although the intensity of the HOPG G-band is less than normally observed (the HOPG G-band intensity is typically comparable to $n \sim 19$ data). As can be seen in the figure, the G-band clearly downshifts with increasing n . Careful Voigt lineshape analyses of these G-bands show that they are extremely well fit by a single Lorentzian that has been “folded” with a Gaussian instrument function. The Gaussian is defined by the spectral shape of the low-pressure Hg line present in all our Raman spectra. Interestingly, the G-band frequency w_G exhibits an almost linear dependence on $1/n$, i.e., $w_G(n) = w_G(8) + b/n$, where $\beta \sim 6 \text{ cm}^{-1}$ is a constant. This behavior is shown in Fig. 4 which presents the results of 8 separate studies (passes) mostly, but not exclusively, obtained from the same set of n GLs. However, in each successive pass, a different location on the particular n GL was excited by the laser.

It is of interest to compare the value obtained for the G-band frequency of SiO_2 -supported graphene, i.e., $w_G(1) = 1587 \text{ cm}^{-1}$ (Fig. 4) to the strongest high frequency 1st order mode of moderate diameter (e.g., $D \sim 1.4 \text{ nm}$) single-walled carbon nanotubes (SWNT), e.g., $\omega \sim 1592 \text{ cm}^{-1}$ ^{19,20,44}. For SWNTs near this diameter (e.g., 1.2 - 1.6 nm), it is thought that the wall curvature of the nanotube does not strongly effect the C-C intra-

atomic force constants^{20, 45}. If we accept this point of view, then our value for $\omega_{G(n=1)} \sim 1587 \text{ cm}^{-1}$ is almost 5 cm^{-1} less than anticipated.

Our Voigt lineshape analysis of the G-bands typically returned an uncertainty for the band frequency of only $\sim 0.1\text{-}0.2 \text{ cm}^{-1}$. Furthermore, absolute frequency calibration uncertainty in our experiments is small ($\sim 0.1\text{-}0.2 \text{ cm}^{-1}$), as all G-band frequency scales are referenced to the nearby Hg line. Thus, it is somewhat surprising that the scatter in the frequency (ω_G) data (Fig. 4) for fixed n is about twice as large as anticipated, i.e., the observed scatter is $\sim \pm 0.5\text{-}1 \text{ cm}^{-1}$. The larger scatter in $\omega_{G(n)}$ data suggests that there may be a spot-to-spot variation within the nGL films. Perhaps this is due to the spectral difference produced by excitation near (or far) from a grain-boundary in the HOPG (the HOPG basal plane grain size is $\sim 1\text{-}3 \mu$ which is comparable to the laser spot diameter).

The symmetry and degeneracy of the long wavelength ($q=0$) optical phonons in graphite and graphene can be obtained by a group theoretical analysis. For graphite, with four atoms per primitive cell (two per layer in adjacent A and B layers), it has been shown that the atomic representation reduces to $\chi_{\text{graphite}} = E_{2g}^{(1)} + E_{2g}^{(2)} + E_{1u} + A_{1u} + B_{1g}$, where the E modes are doubly degenerate, and the A and B modes are singly degenerate. The E_{2g} symmetry modes are Raman-active ($\omega(E_{2g}^{(1)}) = 42 \text{ cm}^{-1}$; $\omega(E_{2g}^{(2)}) = 1582 \text{ cm}^{-1}$). The low frequency $E_{2g}^{(1)}$ modes can be identified with a rigid shearing of adjacent graphene layers²⁰. The low frequency of this mode is a measure of the weak interlayer van der Waals forces. On the other hand, the high frequency Raman-active $E_{2g}^{(2)}$ modes and IR-active E_{1u} (1587 cm^{-1}) modes both involve a stretching of unusually strong *intralayer* bonds; therefore only a small component of the mode restoring force comes from *interlayer* bonds. The out-of-plane graphite A_{1u} (868 cm^{-1}) mode is IR-active and

the B_{1g} mode (127 cm^{-1}) is optically silent. Both the electronic states and the phonon states must depend, to some extent, on n in an n GL. Of course, the question remains: “How much do these states vary with n for small n , and with increasing n , by what value of n will the variation cease to be important”?.

For the case of graphene, there are 2 atoms per primitive cell, and it can be easily shown that $\chi_{\text{graphene}} = E_g + A_1 + B_1$. In graphene, it can then be seen that several “graphitic” modes are lost, i.e., their re-appearance in an n GL requires at least a doubling of the number of layers ($n=2$) and an interlayer interaction. Several calculations of the phonon modes for graphene have appeared^{34-36,46}. Unfortunately, to date, there have not been any experimental reports to test the subtle differences that can occur between the phonons in graphene and graphite. The phonon dispersion and corresponding one-phonon DOS for graphene calculated according to Mapeli and collaborators [ref] appears in Fig. 5. Particular attention in the figure should be paid to strong peaks in the DOS at $\sim 1380 \text{ cm}^{-1}$ and 1600 cm^{-1} and the weak peak at $\sim 1500 \text{ cm}^{-1}$. Evidence for structure in the 1st and 2nd order Raman spectra associated with these maxima are seen, as discussed below

From the symmetry analysis, it should be clear that the Raman band we observe in the interval $\sim 1581\text{-}1588 \text{ cm}^{-1}$ in n GLs (Fig’2 and 3) should be connected with the $E_{2g}^{(2)}$ modes of graphite (G-band), as perturbed by the small number of layers in the film and the coupling of the film to the substrate. However, the one-phonon scattering symmetry analysis does not allow for the weak Raman bands that we observe in n GLs near ~ 1350 , 1450 and 1500 cm^{-1} . These weak Raman bands can be seen in Fig. 6, where we have considerably expanded the intensity so that the G-band maxima are way off-scale. The

strongest band in the figure ($\sim 1350 \text{ cm}^{-1}$) is identified with a “disorder”-induced band or “D-band”, as it is known in the literature, that has been observed in many sp²-bonded carbons. These studies have shown that the Raman D-band intensity and position, respectively, depend on the degree and nature of the basal plane disorder and the excitation wavelength^{20, 31, 47-52}. For the $n=1$ nGL (Fig. 6), we observe that the D-band intensity I_D of the $\sim 1350 \text{ cm}^{-1}$ band is $\sim 1/5$ of that of the G-band (I_G). However, with increasing n , the D-band intensity I_D can be seen to dramatically decline relative to I_G . We observe that the intensity ratio (I_D/I_G) exhibits an approximately exponential decline with increasing n . In addition to the $\sim 1350 \text{ cm}^{-1}$ D-band, two additional weak bands are observed that are also assigned to disorder-induced 1st order scattering or “D-scattering”: (D_2) $\sim 1450 \text{ cm}^{-1}$ and (D_3) 1500 cm^{-1} . It should be noted that the graphene phonon calculations of Mapeli et al. predict a weak but sharp DOS peak at $\sim 1500 \text{ cm}^{-1}$. This 1500 cm^{-1} peak is particularly interesting in that it has striking n -dependence, whereas the other D-scattering peaks (e.g., $D_2 \sim 1350 \text{ cm}^{-1}$ and $D_3 \sim 1450 \text{ cm}^{-1}$) are largely insensitive to n .

It is also interesting to speculate about the origin of the n -dependence of the D-band scattering in nGLs. One explanation that we might offer for this observation is a bending of the graphene layers necessary to accommodate the surface roughness of the substrate. This view is motivated by the fact that our SiO₂:Si substrates are not atomically smooth. Our AFM measurements indicate a substrate roughness of $\sim 1-2 \text{ nm}$, i.e., $\sim 3-6$ graphene layers. The n -dependence of the D-scattering then may stem from the loss in sp² bond bending disorder associated with the increase in rigidity of the nGL as the number of layers n increases. This cooperative (multilayer) film rigidity is expected to resist the deformation from planarity as the film, via a van der Waals coupling between substrate

and n GL, attempts to conform to the underlying substrate roughness. That is, an $n=1$ n GL is relatively very compliant and bends easily, while an $n=5$ n GL should be much more rigid. Our suggestion of a planar deformation to induce D-band scattering, although novel, is consistent with the general concept that many different mechanisms that break the translational symmetry of the basal plane can give rise to D-band scattering (e.g., finite basal plane size, boron-doping, bond-disorder, etc.)^{31, 47-53}. Further work will be needed to confirm that variable film rigidity is responsible for the D-band scattering. This idea could be experimentally tested by studying films supported on atomically smooth substrates (e.g., mica) or suspended over a small hole in a substrate.

In Fig. 7, we display in three separate panels, the 2nd order features shown in Fig. 2, but on an expanded intensity scales. For clarity, the spectra are normalized to give them all approximately the same intensity, independent of n . The panels each display the evolution ($n=1$ (bottom) to HOPG (top)) of one of the three 2nd order bands observed at: $\sim 2450 \text{ cm}^{-1}$ (weak intensity), $\sim 2700 \text{ cm}^{-1}$ (moderate to strong intensity) and $\sim 3248 \text{ cm}^{-1}$ (moderate intensity). Based on the peaks in the phonon DOS of Mapeli et al. (Fig. 5), the $\sim 2450 \text{ cm}^{-1}$ and $\sim 2700 \text{ cm}^{-1}$ bands must be due to combination scattering, i.e., $(\omega_1 + \omega_2)$, while the relatively narrow 2nd order band at $\sim 3248 \text{ cm}^{-1}$ must be a 2ω feature (overtone scattering) associated with a doubling of the highest phonon frequency in the zone. It is interesting that although we observe that the G-band ($q=0$ mode of this optical branch) upshifts with decreasing n , while the maximum frequency of the same branch $\omega(\text{max})$ remains fixed in frequency. This result, amongst other experimental observations presented here, seems to be a good test for future lattice dynamics models of n GLs and *supported* n GLs..

In summary, we have prepared a variety of ultrathin graphitic films (or n GLs) by mechanical transfer from an HOPG slab to a SiO_2/Si substrate. The film thickness of various n GL flakes was measured by averaging AFM z-scans. They exhibited lateral dimensions on the order of ~ 2 - 5 microns. The effective film thickness data h vs. *assigned* n was found to be well fit to a straight line, yielding the value $t=0.355$ for the thickness of a graphene layer, a little larger than $c/2$ for graphite, but within experimental error. MicroRaman spectra were then collected on these films and correlated with the integer number of graphene layers per film. Surprisingly, despite the anticipated short range of the c -axis forces in graphite, the Raman spectra of n GLs were found to be very sensitive to n , for n as large as $n=10$. Strong signatures of the number of graphene layers per film are seen in the weak D_3 -scattering peak at $\sim 1500 \text{ cm}^{-1}$, in the position of the G-band, and in the 2nd order band observed near $\sim 2700 \text{ cm}^{-1}$. Detailed lattice dynamics calculations should be carried out on atomically thin films (vs. n) to understand how the subtle changes we observe in zone-center, mid-zone and zone edge modes affect the D, 1st and 2nd order scattering. It will also be necessary to extend these experimental studies to other excitation wavelengths (λ_{ex}) to see which of these Raman bands are dispersive (i.e., the position of dispersive Raman bands depends on λ_{ex}). The simple $1/n$ behavior of the G-band position also remains unexplained. It is not known to what extent the $1/n$ dependence is connected to strain (via coupling to the substrate) or to the finite number n of C-layers in the film.

Finally, the n GL D-band scattering intensity ($\sim 1350 \text{ cm}^{-1}$) is observed to strongly decrease with increasing n . We have proposed that this behavior might correlate with the

rigidity of the film and its ability to avoid distortion to accommodate the substrate roughness.

Acknowledgements: This work was supported, in part, by Penn State Materials Research Institute and the Penn State MRSEC under NSF grant DMR 0213623. Authors acknowledge useful discussion with Dr. Humberto R. Gutierrez (Penn State) and Cynthia Coggins (PSIA, Inc.)

Figure captions

Fig. 1. Effective n GL film height vs. assigned n . The straight line is a least square fit to the data. The apparent thickness of a graphene layer is $t=0.35\pm 0.01$ nm, and the AFM offset parameter is $t_0=0.33$ nm (see text for discussion).

Fig. 2. High-frequency 1st and 2nd order microRaman spectra of n GL films supported on a SiO₂:Si substrate and HOPG. The data were collected using 514.5 nm radiation under ambient conditions. The spectra are scaled to produce an approximate match in intensity for the ~ 2700 cm⁻¹ band. Note: (1) the shape and frequency of this 2nd order band is sensitive to the number of layers n and (2) the relative intensity of the 2nd order band at 2700 cm⁻¹ is larger than the 1st order-allowed G-band for $n < 5$.

Fig. 3. 1st order-allowed Raman G-band for supported n GL films vs. number of layers n . The data were collected using 514.5 nm radiation under ambient conditions. The position of this band upshifts linearly relative to graphite with increasing $1/n$ (see Fig. 4).

Fig. 4. G-band frequency vs. $1/n$. Each pass represents a set of data collected under identical optical conditions. The solid line represents the results of a least squares fit to the data: $\omega_G(\text{infinity})=1581.6$ cm⁻¹ and $d\omega/d(1/n)=5.5$ cm⁻¹. The average of five values found for supported graphene ($n=1$) is $\omega_G=1587.1$ cm⁻¹.

Fig. 5. Calculated phonon dispersion curves and one-phonon density of states (DOS) for unsupported (free standing) graphene by Mapeli et al.⁴⁶. Structure in the phonon DOS is expected in D- and 2nd order-scattering.

Fig. 6. Raman spectra (expanded intensity scale) of supported n GL films and HOPG in the vicinity of the G-band. The data were collected using 514.5 nm radiation under ambient conditions. The spectra have been scaled to show the weak structure which has been identified with the one-phonon DOS in Fig. 5. The arrows in the figure identify weak scattering features. Note that the D₃ feature at ~ 1500 cm⁻¹ is sensitive to the number of layers n .

Fig. 7 2nd order Raman spectra of supported n GL films. The data were collected using 514.5 nm radiation under ambient conditions. The spectra in each panel have been scaled to generate features of approximately the same height. These 2nd order bands also appear in Fig. 2 which indicates their approximate relative scattering intensity to the G-band. Note that the ~ 2700 cm⁻¹ band is sensitive to the number of layers n .

References

1. Bunch, J. S.; Yaish, Y.; Brink, M.; Bolotin, K.; McEuen, P. L., Coulomb oscillations and Hall effect in quasi-2D graphite quantum dots. *Nano Letters* **2005**, 5, (2), 287.
2. Dujardin, E.; Thio, T.; Lezec, H.; Ebbesen, T. W., Fabrication of mesoscopic devices from graphite microdisks. *Applied Physics Letters* **2001**, 79, (15), 2474.
3. Kempa, H.; Semmelhack, H. C.; Esquinazi, P.; Kopelevich, Y., Absence of metal-insulator transition and coherent interlayer transport in oriented graphite in parallel magnetic fields. *Solid State Communications* **2003**, 125, (1), 1.
4. Kopelevich, Y.; Torres, J. H. S.; da Silva, R. R.; Mrowka, F.; Kempa, H.; Esquinazi, P., Reentrant metallic behavior of graphite in the quantum limit. *Physical Review Letters* **2003**, 90, (15), 156402/1.
5. Novoselov, K. S.; Geim, A. K.; Morozov, S. V.; Jiang, D.; Katsnelson, M. I.; Grigorieva, I. V.; Dubonos, S. V.; Firsov, A. A., Two-dimensional gas of massless Dirac fermions in graphene. *Nature (London, United Kingdom)* **2005**, 438, (7065), 197.
6. Novoselov, K. S.; Geim, A. K.; Morozov, S. V.; Jiang, D.; Zhang, Y.; Dubonos, S. V.; Grigorieva, I. V.; Firsov, A. A., Electric field effect in atomically thin carbon films. *Science* **2004**, 306, (5696), 666.
7. Novoselov, K. S.; McCann, E.; Morozov, S. V.; Falko, V. I.; Katsnelson, M. I.; Geim, A. K.; Schedin, F.; Jiang, D., Unconventional quantum Hall effect and Berry's phase of 2p in bilayer graphene. *Los Alamos National Laboratory, Preprint Archive, Condensed Matter* **2006**, 1.
8. Zhang, Y.; Jiang, Z.; Small, J. P.; Purewal, M. S.; Tan, Y. W.; Fazlollahi, M.; Chudow, J. D.; Jaszczak, J. A.; Stormer, H. L.; Kim, P., Landau level splitting in graphene in high magnetic fields. *Los Alamos National Laboratory, Preprint Archive, Condensed Matter* **2006**, 1.
9. Zhang, Y.; Tan, Y.-W.; Stormer, H. L.; Kim, P., Experimental observation of the quantum Hall effect and Berry's phase in graphene. *Nature (London, United Kingdom)* **2005**, 438, (7065), 201.
10. Zhang, Y. B.; Small, J. P.; Amori, M. E. S.; Kim, P., Electric field modulation of galvanomagnetic properties of mesoscopic graphite. *Physical Review Letters* **2005**, 94, (17), 176803/1.
11. Zhang, Y. B.; Small, J. P.; Pontius, W. V.; Kim, P., Fabrication and electric-field-dependent transport measurements of mesoscopic graphite devices. *Applied Physics Letters* **2005**, 86, (7), 073104.
12. Ohashi, Y.; Yamamoto, K.; Kubo, T., Shubnikov-de Haas effect of very thin graphite crystals. *Carbon'01, An International Conference on Carbon, Lexington, KY, United States, July 14-19, 2001* **2001**, 568.
13. Ohashi Y., Y. K., Kubo T., Magnetoresistance effect of thin films made of single graphite crystal. *Tanso* **2000**, 195, 410.
14. Berger, C.; Song, Z.; Li, T.; Li, X.; Ogbazghi, A. Y.; Feng, R.; Dai, Z.; Marchenkov, A. N.; Conrad, E. H.; First, P. N.; de Heer, W. A., Ultrathin epitaxial graphite: two-dimensional electron gas properties and a route toward graphene-based nanoelectronics. *Journal of Physical Chemistry B* **2004**, 108, (52), 19912.
15. Rollings, E.; Gweon, G. H.; Zhou, S. Y.; Mun, B. S.; Hussain, B. S.; Fedorov, A. V.; First, P. N.; de Heer, W. A.; Lanzara, A., Synthesis and characterization of atomically-thin graphite films on a silicon carbide substrate. *Los Alamos National Laboratory, Preprint Archive, Condensed Matter* **2005**, 1.
16. Morozov, S. V.; Novoselov, K. S.; Schedin, F.; Jiang, D.; Firsov, A. A.; Geim, A. K., Two-dimensional electron and hole gases at the surface of graphite. *Physical Review B: Condensed Matter and Materials Physics* **2005**, 72, (20), 201401/1.
17. Novoselov, K. S.; Geim, A. K.; Morozov, S. V.; Jiang, D.; Katsnelson, M. I.; Grigorieva, I. V.; Dubonos, S. V.; Firsov, A. A., Two-dimensional gas of massless Dirac fermions in graphene. *Nature* **2005**, 438, (7065), 197.
18. Gusynin, V. P.; Sharapov, S. G., Unconventional Integer Quantum Hall Effect in Graphene. *Physical Review Letters* **2005**, 95, (14), 146801/1.
19. Dresselhaus, M. S.; Dresselhaus, G.; Eklund, P. C.; Editors, *Science of Fullerenes and Carbon Nanotubes*. 1996; p 965.
20. Dresselhaus, M. S.; Eklund, P. C., Phonons in carbon nanotubes. *Advances in Physics* **2000**, 49, (6), 705.
21. Chico, L.; Perez-Alvarez, R.; Cabrillo, C., Low-frequency phonons in carbon nanotubes: A continuum approach. *Physical Review B* **2006**, 73, (7).
22. Maultzsch, J.; Reich, S.; Schlecht, U.; Thomsen, C., High-energy phonon branches of an individual metallic carbon nanotube. *Physical Review Letters* **2003**, 91, (8).
23. Maultzsch, J.; Reich, S.; Thomsen, C.; Dobardzic, E.; Milosevic, I.; Damnjanovic, M., Phonon dispersion of carbon nanotubes. *Solid State Communications* **2002**, 121, (9-10), 471.
24. Maultzsch, J.; Reich, S.; Thomsen, C.; Requardt, H.; Ordejon, P., Phonon dispersion in graphite. *Physical Review Letters* **2004**, 92, (7).

25. Saito, R.; Jorio, A.; Souza, A. G.; Dresselhaus, G.; Dresselhaus, M. S.; Pimenta, M. A., Probing phonon dispersion relations of graphite by double resonance Raman scattering. *Physical Review Letters* **2002**, 88, (2).
26. Saito, R.; Takeya, T.; Kimura, T.; Dresselhaus, G.; Dresselhaus, M. S., Raman intensity of single-wall carbon nanotubes. *Physical Review B* **1998**, 57, (7), 4145.
27. Wirtz, L.; Rubio, A., The phonon dispersion of graphite revisited. *Solid State Communications* **2004**, 131, (3-4), 141.
28. Yu, J.; Kalia, R. K.; Vashishta, P., Phonons in Graphitic Tubules - a Tight-Binding Molecular-Dynamics Study. *Journal of Chemical Physics* **1995**, 103, (15), 6697.
29. Zolyomi, V.; Kurti, J.; Gruneis, A.; Kuzmany, H., Origin of the fine structure of the Raman D band in single-wall carbon nanotubes. *Physical Review Letters* **2003**, 90, (15).
30. Aljishi, R.; Dresselhaus, G., Lattice-Dynamical Model for Graphite. *Physical Review B* **1982**, 26, (8), 4514.
31. Ferrari, A. C.; Robertson, J., Interpretation of Raman spectra of disordered and amorphous carbon. *Physical Review B* **2000**, 61, (20), 14095.
32. Nicklow, R.; Smith, H. G.; Wakabaya, N., Lattice-Dynamics of Pyrolytic-Graphite. *Physical Review B* **1972**, 5, (12), 4951.
33. Nicklow, R.; Wakabaya, N.; Smith, H. G., Lattice Dynamics of Pyrolytic Graphite. *Bulletin of the American Physical Society* **1970**, 15, (3), 383.
34. Yanagisawa, H.; Tanaka, T.; Ishida, Y.; Matsue, M.; Rokuta, E.; Otani, S.; Oshima, C., Analysis of phonons in graphene sheets by means of HREELS measurement and ab initio calculation. *Surface and Interface Analysis* **2005**, 37, (2), 133.
35. Popov, V. N.; Lambin, P., Radius and chirality dependence of the radial breathing mode and the G-band phonon modes of single-walled carbon nanotubes. *Physical Review B* **2006**, 73, (8), 085407.
36. Saito, R.; Takeya, T.; Kimura, T.; Dresselhaus, G.; Dresselhaus, M. S., Finite-size effect on the Raman spectra of carbon nanotubes. *Physical Review B* **1999**, 59, (3), 2388.
37. Novoselov, K. S.; Jiang, D.; Schedin, F.; Booth, T. J.; Khotkevich, V. V.; Morozov, S. V.; Geim, A. K., Two-dimensional atomic crystals. *Proceedings of the National Academy of Sciences of the United States of America* **2005**, 102, (30), 10451.
38. Gupta, A.; Joshi, P.; Eklund, P. C. In *Raman Scattering from few-layer Graphene Films*, 2006 APS March Meeting, Baltimore, MD, 2006; Baltimore, MD, 2006.
39. Moore, A. W., Properties and applications of highly oriented pyrolytic graphite - a review. *Extended Abstracts and Program - Biennial Conference on Carbon* **1979**, 14, 203.
40. Moore, A. W., Highly oriented pyrolytic graphite. *Chemistry and Physics of Carbon* **1973**, 11, 69.
41. Xiang, J.; Lu, W.; Hu, Y. J.; Wu, Y.; Yan, H.; Lieber, C. M., Ge/Si nanowire heterostructures as high-performance field-effect transistors. *Nature* **2006**, 441, (7092), 489.
42. Tans, S. J.; Verschueren, A. R. M.; Dekker, C., Room-temperature transistor based on a single carbon nanotube. *Nature* **1998**, 393, (6680), 49.
43. Kelly, B. T., *Physics of graphite*. Applied Science: London, 1981.
44. Rao, A. M.; Richter, E.; Bandow, S.; Chase, B.; Eklund, P. C.; Williams, K. A.; Fang, S.; Subbaswamy, K. R.; Menon, M.; Thess, A.; Smalley, R. E.; Dresselhaus, G.; Dresselhaus, M. S., Diameter-selective Raman scattering from vibrational modes in carbon nanotubes. *Science* **1997**, 275, (5297), 187.
45. Jishi, R. A.; Venkataraman, L.; Dresselhaus, M. S.; Dresselhaus, G., Phonon Modes in Carbon Nanotubes. *Chemical Physics Letters* **1993**, 209, (1-2), 77.
46. Mapelli, C.; Castiglioni, C.; Zerbi, G.; Mullen, K., Common force field for graphite and polycyclic aromatic hydrocarbons. *Physical Review B* **1999**, 60, (18), 12710.
47. Brown, S. D. M.; Jorio, A.; Dresselhaus, M. S.; Dresselhaus, G., Observations of the D-band feature in the Raman spectra of carbon nanotubes. *Physical Review B* **2001**, 64, (7), 073403.
48. Dresselhaus, M. S.; Dresselhaus, G.; Jorio, A.; Souza, A. G.; Pimenta, M. A.; Saito, R., Single nanotube Raman spectroscopy. *Accounts of Chemical Research* **2002**, 35, (12), 1070.
49. Jorio, A.; Pimenta, M. A.; Fantini, C.; Souza, M.; Souza, A. G.; Samsonidze, G. G.; Dresselhaus, G.; Dresselhaus, M. S.; Saito, R., Advances in single nanotube spectroscopy: Raman spectra from cross-polarized light and chirality dependence of Raman frequencies. *Carbon* **2004**, 42, (5-6), 1067.
50. Liu, C. P.; Ding, J. W., Electronic structure of carbon nanotube: the roles of curvature, hybridization, and disorder. *Journal of Physics-Condensed Matter* **2006**, 18, (16), 4077.
51. Moradian, R., Disordered carbon nanotube alloys in the effective-medium supercell approximation. *Physical Review B* **2004**, 70, (20).
52. Pimenta, M. A.; Jorio, A.; Brown, S. D. M.; Souza, A. G.; Dresselhaus, G.; Hafner, J. H.; Lieber, C. M.; Saito, R.; Dresselhaus, M. S., Diameter dependence of the Raman D-band in isolated single-wall carbon nanotubes. *Physical Review B* **2001**, 64, (4).
53. Dresselhaus, M. S.; Dresselhaus, G.; Pimenta, M. A.; Eklund, P. C., Raman Scattering in Carbon Materials. In *Analytical Applications of Raman Spectroscopy*, Pelletier, M. J., Ed. Blackwell Science Ltd. : Oxford, UK, 1999; pp 367.

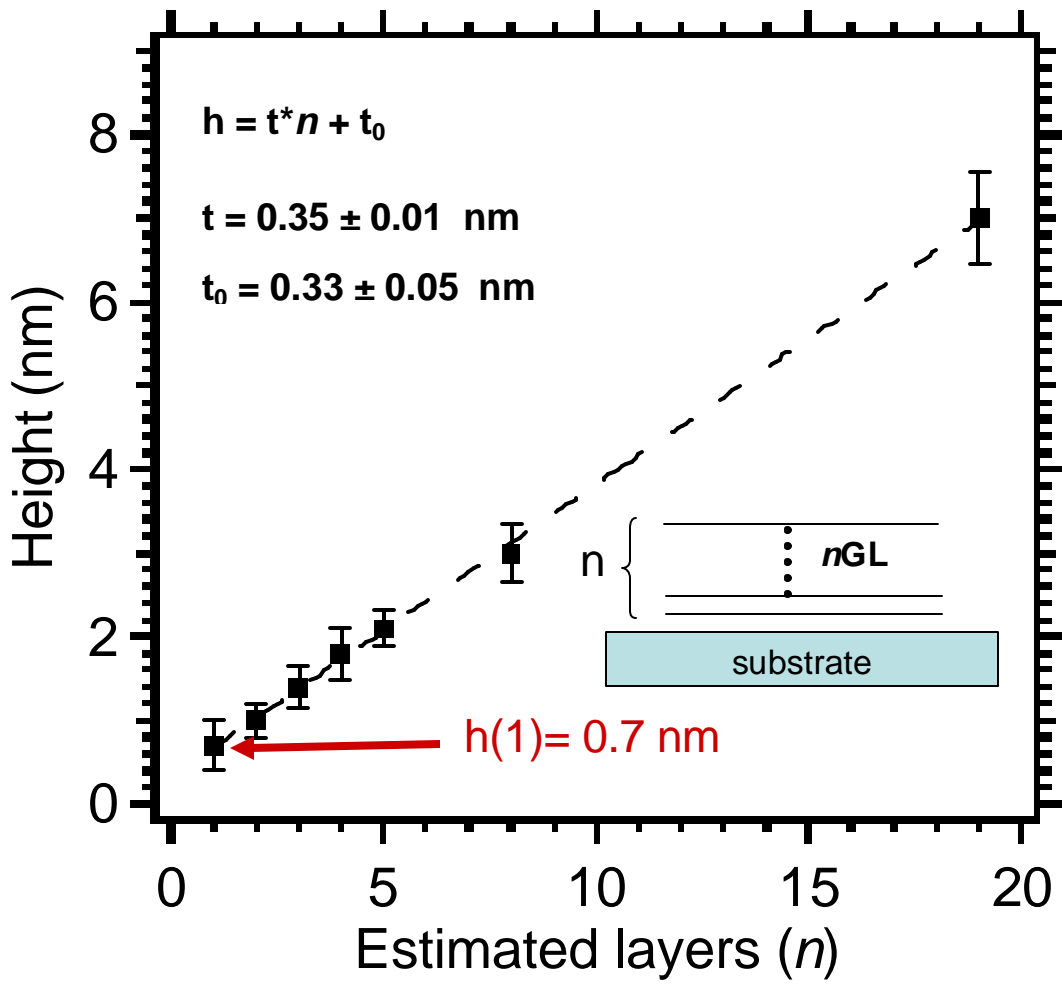


Fig. 1

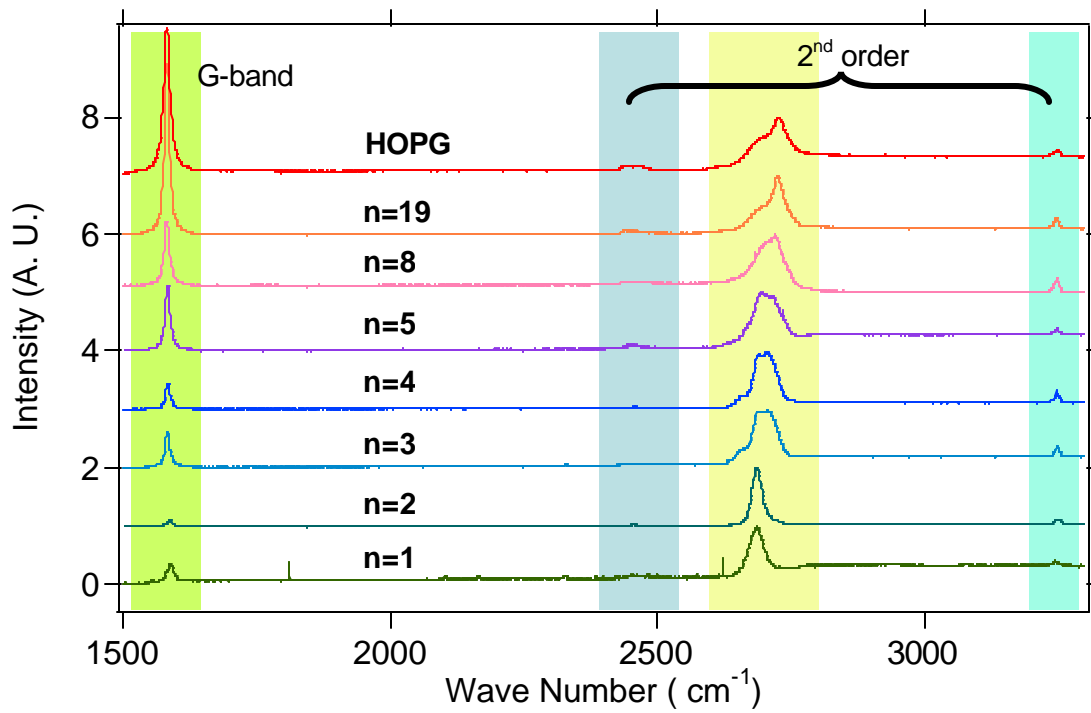


Fig. 2

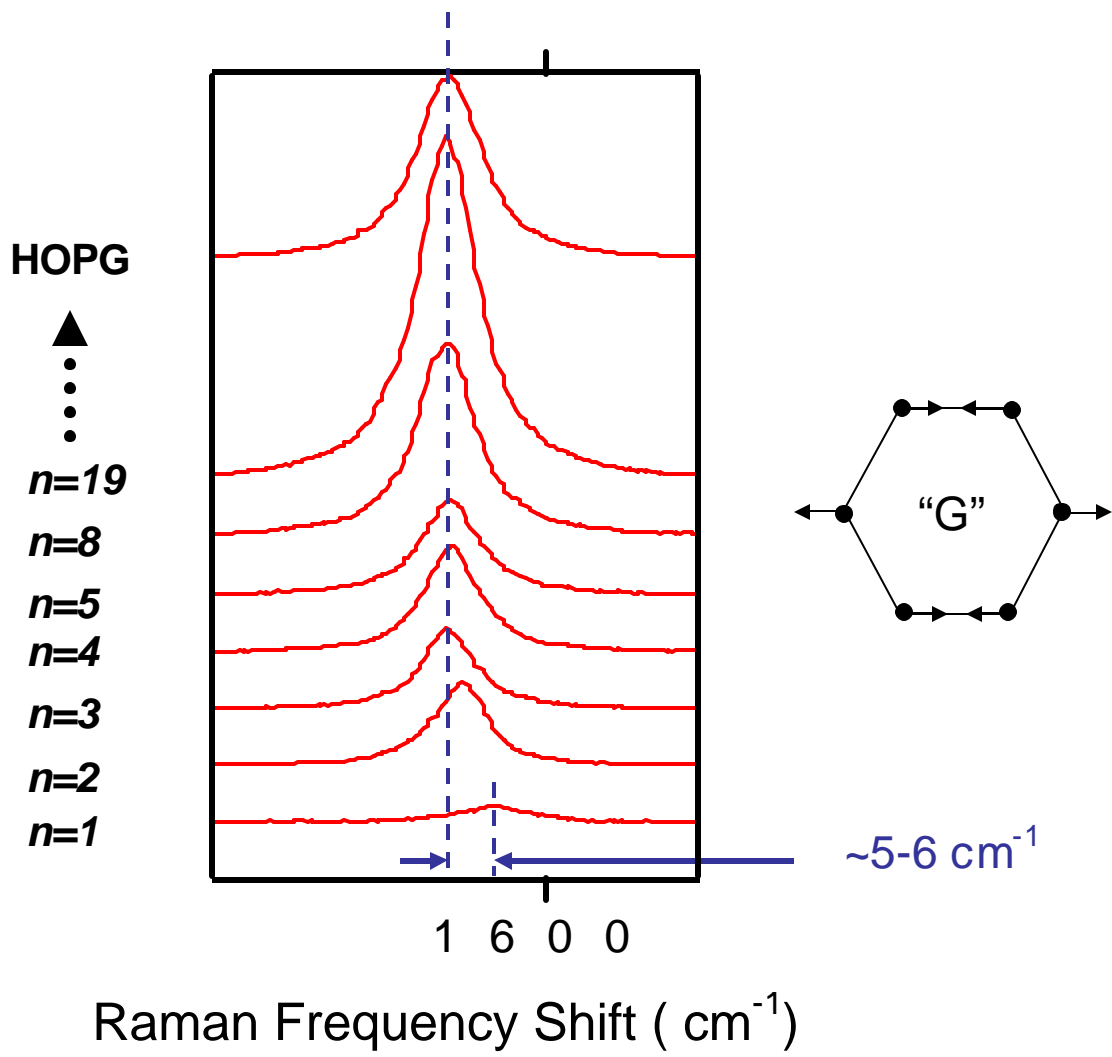


Fig. 3

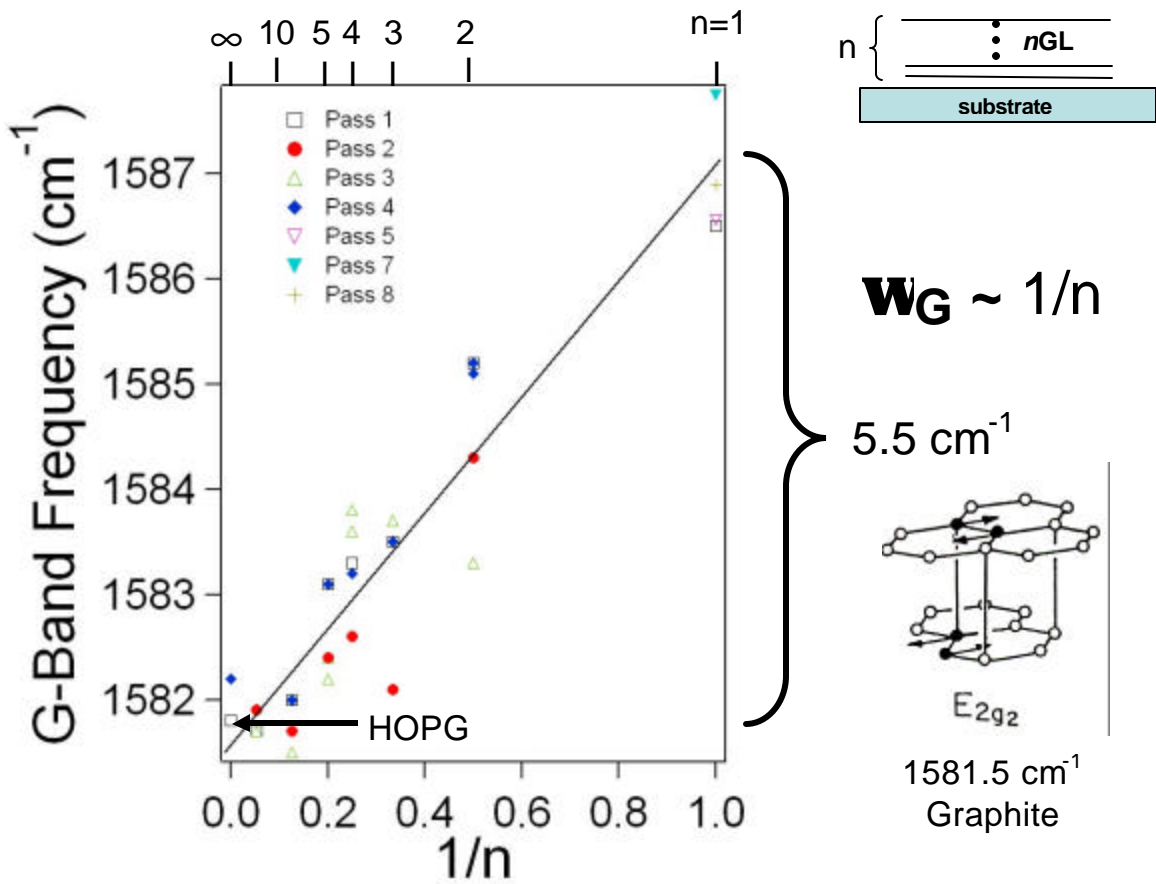


Fig. 4

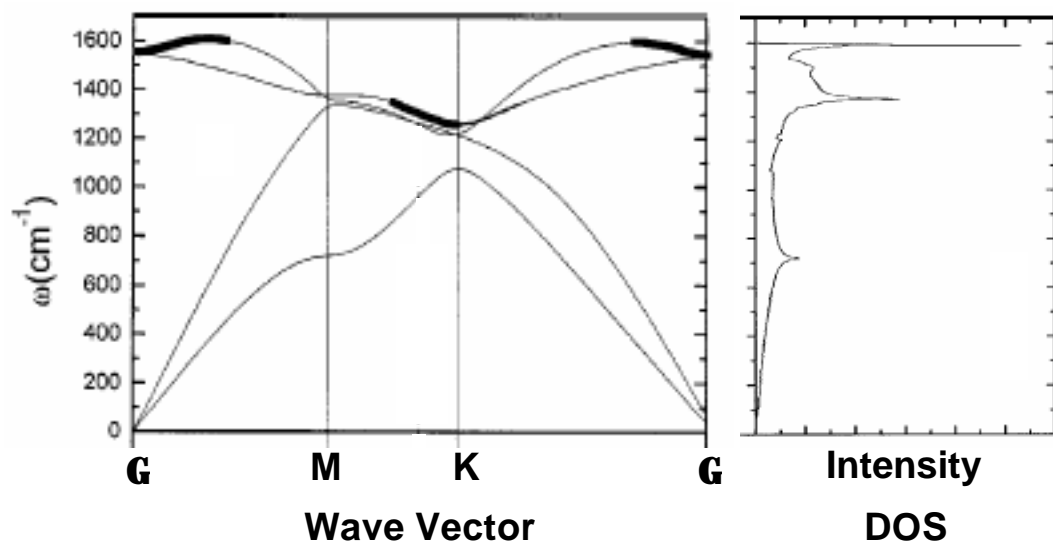


Fig. 5

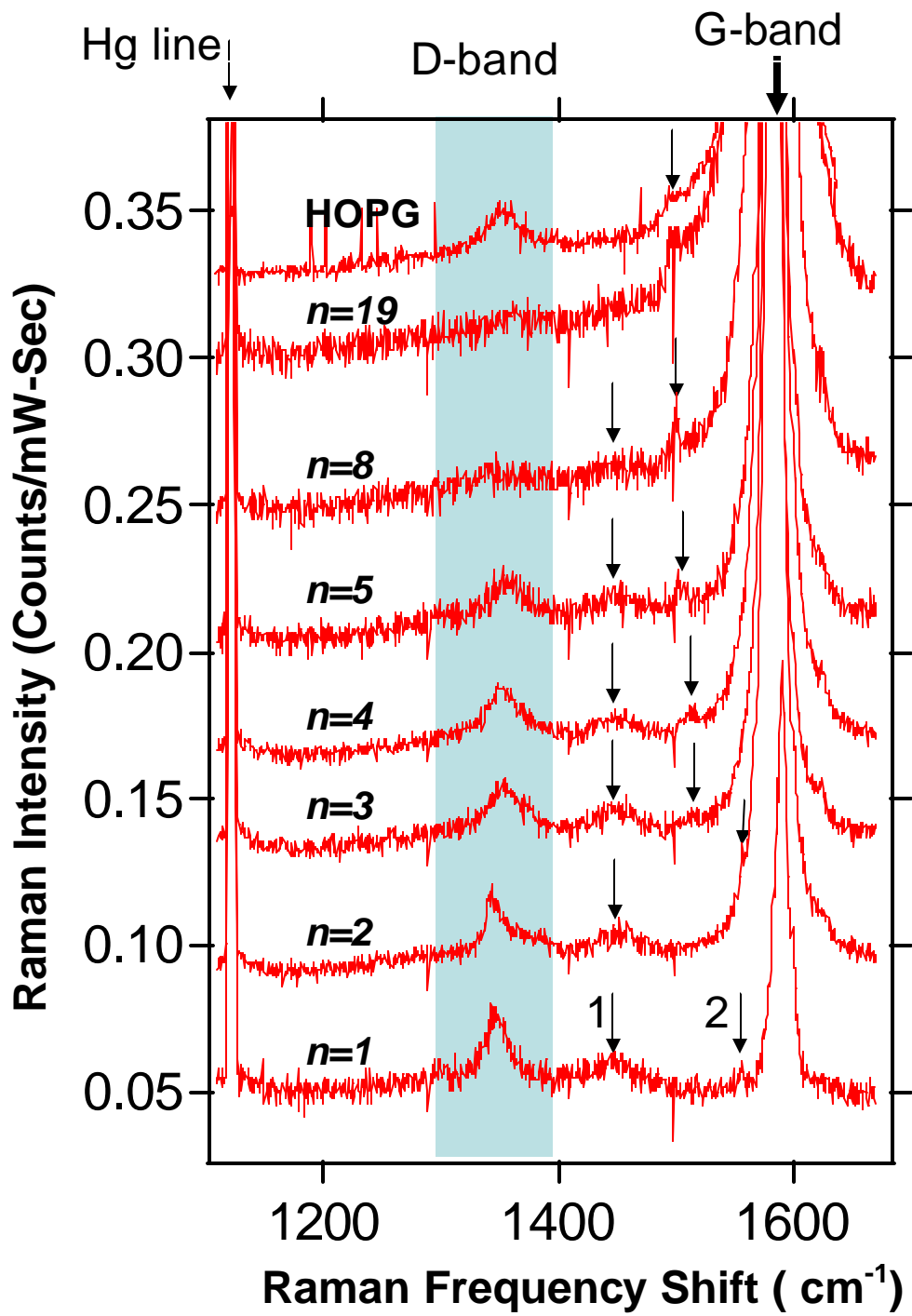


Fig. 6

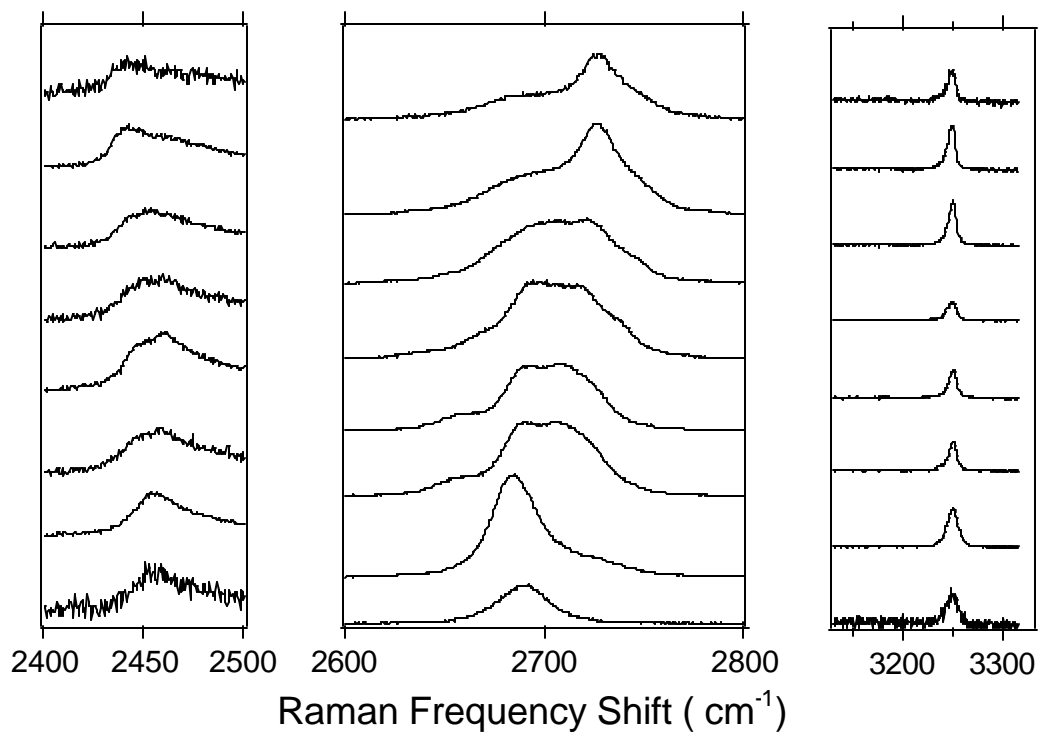


Fig. 7